

Detecting high- z galaxies in the Near Infrared Background

Bin Yue¹, Andrea Ferrara^{1,2}, Kári Helgason³

¹*Scuola Normale Superiore, Piazza dei Cavalieri 7, I-56126 Pisa, Italy*

²*Kavli IPMU (WPI), Todai Institutes for Advanced Study, The University of Tokyo, 5-1-5 Kashiwanoha, Kashiwa 277-8583, Japan*

³*Max Planck Institute for Astrophysics, Karl-Schwarzschild-Str. 1, 85748 Garching, Germany*

22 March 2021

ABSTRACT

Emission from high- z galaxies must unquestionably contribute to the near-infrared background (NIRB). However, this contribution has so far proven difficult to isolate even after subtracting the resolved galaxies to deep levels. Remaining NIRB fluctuations are dominated by unresolved low- z galaxies on small angular scales, and by an unidentified component with unclear origin on large scales ($\approx 1000''$). In this paper, by analyzing mock maps generated from semi-numerical simulations and empirically determined $L_{UV} - M_h$ relations, we find that fluctuations associated with galaxies at $5 < z < 10$ amount to several percent of the unresolved NIRB flux fluctuations. We investigate the properties of this component for different survey areas and limiting magnitudes. In all cases, we show that this signal can be efficiently, and most easily at small angular scales, isolated by cross-correlating the source-subtracted NIRB with Lyman Break Galaxies (LBGs) detected in the same field by HST surveys. This result provides a fresh insight into the properties of reionization sources.

Key words: cosmology: diffuse radiation-dark ages; reionization, first stars – infrared:diffuse-background – galaxies: high-redshift

1 INTRODUCTION

The cosmic infrared background (CIB or CIRB) contains a considerable fraction of the collective radiation emitted by stars through the cosmic time. Stars in the Epoch of Reionization (EoR) have the bulk of their radiation redshifted into the near-infrared band ($\sim 0.7 - 5 \mu\text{m}$) and the CIB measured in this band is specifically named “near-infrared background” (NIRB). As such, the NIRB offers a unique opportunity to study faint high- z galaxies that remain largely undetected in deep galaxy surveys (see e.g. Salvaterra & Ferrara 2006; Fernandez & Komatsu 2006; Fernandez et al. 2010, 2012, 2013; Fernandez & Zaroubi 2013). This is particularly important as these objects are commonly believed to provide most of the ionizing power that drives cosmic reionization (Choudhury & Ferrara 2007; Raičević et al. 2011; Salvaterra et al. 2011). Besides, the NIRB might also help characterizing the stellar populations of the first cosmic systems (Salvaterra & Ferrara 2003; Salvaterra et al. 2006; Santos et al. 2002; Kashlinsky et al. 2004, 2005; Magliocchetti et al. 2003; Cooray & Yoshida 2004; Cooray et al. 2004).

Most recent studies have converged on the prediction that on scales of $\approx 1000''$ the fluctuation level from normal star-forming galaxies at $z \gtrsim 5$ is $\approx 10^{-3} \text{ nWm}^{-2}\text{sr}^{-1}$ at $3.6 \mu\text{m}$ (Cooray et al. 2012a; Yue et al. 2013a; Helgason et al. 2016). However, extracting such sig-

nal from available data has been so far very challenging, as even when the deepest galaxy subtraction from NIRB maps is applied, the remaining flux fluctuations¹ still cannot be ascribed to the known high- z galaxy population. On small angular scales, most of the signal arises from unresolved low- z galaxies (see the first analysis by Kashlinsky et al. 2002). On larger scales the measured power (see e.g. Kashlinsky et al. 2004, 2005, 2007c,b, 2012; Matsumoto et al. 2005, 2011; Seo et al. 2015; Cooray et al. 2007, 2012b) is $\gtrsim 100$ times larger than the low- z galaxies (Helgason et al. 2012), and $\gtrsim 1000$ times larger than that expected from high- z normal star-forming galaxies and first stars (Cooray et al. 2012a; Yue et al. 2013a). Therefore it must be attributed to some, yet unknown, alternative sources. Basically, two different explanations have been proposed for the origin of such large scale ($\sim 1000''$) “power excess”. They involve either early accreting black holes (Yue et al. 2013b, 2014) which could explain the detected NIRB-cosmic X-ray background coher-

¹ NIRB studies usually concentrate on fluctuations rather than absolute flux, as the latter is difficult to measure due to the presence of an overwhelming foreground. However, as the foreground is rather smooth on scales at which the NIRB is measured, the fluctuations analysis is more robust – see e.g. Thompson et al. 2007; Matsumoto et al. 2011; Kashlinsky et al. 2012; Cooray et al. 2012b.

ence (Cappelluti et al. 2013), or “intrahalo light” that radiated by stars ejected from their parent galaxies during merger events (Cooray et al. 2012b; Zemcov et al. 2014).

At present it is unclear which hypothesis should be preferred. Besides, it is also possible that first stars or black holes are much more abundant than in the standard theoretical framework – for example if the slope of the density fluctuations power spectrum slightly deviates from the standard one, the number of small halos (thus stars or black holes therein) could be boosted exponentially – they can then provide sufficient radiation power. To be consistent with electron scattering reionization bounds, at the same time the ionizing photon escape probability must be rather low (for a detailed discussion see Helgason et al. 2016). To further complicate the interpretation, recent observations (Zemcov et al. 2014) show that, on large scales and at least for the 1.1 and 1.6 μm bands, diffuse Galactic light (DGL) might provide a non-negligible flux contribution. However Kashlinsky et al. (2007b) (see Arendt et al. 2010 as well) found that at the 3.6 and 4.5 μm bands the DGL or the Galactic cirrus component is largely subdominant.

For the above reasons, it is urgent to devise new strategies that put our understanding on firmer grounds. In order to isolate the signal from increasingly high redshifts, with sufficient depth and angular resolution one can in principle remove foreground galaxies down to extremely faint levels. This is challenging for current instrumentation, and also not an easy task for the *JWST*, as the signal from high- z galaxies is expected to be subdominant even at ~ 32 AB mag (Helgason et al. 2016). Alternatively, cross-correlation studies seem promising. The NIRB-HI 21cm line cross-correlation (Fernandez et al. 2014; Mao 2014) has the advantage that it selectively picks up the signal from reionization sources. Also, the NIRB, if produced by sources in the EoR, would be cross-correlated with the CMB through the thermal Sunyaev-Zeldovich effect. This correlation could be seen in the forthcoming Euclid-based all-sky CIB maps (Atrio-Barandela & Kashlinsky 2014). In addition to cross-correlation, a recent work (Kashlinsky et al. 2015) proposed the use of Lyman-break tomography to constrain the NIRB contribution from sources above a certain redshift.

Kashlinsky et al. (2007a) analyzed the cross-correlation between the ACS-detected faint sources and the source-subtracted NIRB. They found significant correlation on small scales, implying that the faint ACS galaxies do contribute to NIRB fluctuations. However, these sources (or objects associated with them) cannot account for the large scale clustering as the measured correlation is negligible. Their analysis did not pay particular attention to the high- z sources, therefore the information on high- z galaxies cannot be directly derived from there. It is surprising that so far little attention has been devoted to the search for high- z normal star-forming galaxy signatures in the NIRB, given that deep galaxy surveys have made tremendous progresses in obtaining the UV luminosity functions (LF) up to $z = 10$ (Bouwens et al. 2015), and the detection limits of Lyman break galaxy (LBG) surveys carried out by *HST* have already reached $H \sim 29 - 31$ (Illingworth et al. 2013; Bouwens et al. 2011). Measuring their intensity fluctuations present (though tiny) in the NIRB is essentially one of the most exciting perspectives as it might convincingly show that NIRB fluctuation experiments can be used to study

the first galaxies. Such an experiment is also complementary to more traditional galaxy surveys that derive the LF of the brightest galaxies among early populations.

In summary, it is mandatory to show that the NIRB power spectrum signal of already known high- z galaxies can be recovered robustly. Demonstrating a successful strategy will represent a major step forward in the methodology and allows to obtain, in addition to the clustering signal, other key quantities, as e.g. the colors of high- z galaxies beyond the observed H band. Colors, in turn, provide potentially information on stellar ages and initial mass function of the stars harbored by galaxies in the EoR.

The idea we propose here is to isolate the targeted LBG signal and show the feasibility of statistically detecting reionization sources by cross-correlating deep LBG surveys with NIRB maps. To this aim, we: (a) construct large scale mock maps of the source-subtracted NIRB and LBG catalogs using semi-numerical simulations; (b) perform a cross-correlation analysis between the two data sets to extract the contribution of high- z galaxies in the NIRB. The paper is organized as follows. In Sec. 2 we describe the steps to construct the mock maps. In Sec. 3 we present the analysis about the correlation coefficient and the colors. Conclusions and discussions are presented in Sec. 4. Throughout this paper we use **Planck** cosmological parameters: $\Omega_m = 0.31, \Omega_\Lambda = 0.69, \Omega_b = 0.048, n_s = 0.96, \sigma_8 = 0.82$ and $h = 0.68$ (Planck Collaboration et al. 2014). All magnitudes are in the AB-system (Oke & Gunn 1983).

2 CONSTRUCTION OF MOCK MAPS

2.1 High- z galaxies

Using the code **DexM**² (Mesinger & Furlanetto 2007) we carry out semi-numerical simulations to get catalogs of halos with mass $M_h \gtrsim 5 \times 10^8 M_\odot$ from $z = 5$ to 10 for every $\Delta z = 0.1$. We adopt a 400 Mpc box size that corresponds to an angular size of ≈ 2.4 deg at $z = 10$. We construct a cuboid by replicating the output boxes along the line-of-sight, adding random translations, rotations and reflections (Blaizot et al. 2005). This is our light-cone since we assume that all lines-of-sight are parallel – an assumption that is convenient and safe enough when $z \gtrsim 5$.

To construct flux maps from the light-cone, we link galaxy luminosities to halo mass M_h . The observed LFs could be reproduced exactly if we derive the $L_{UV} - M_h$ relation through abundance matching, i.e. we force the number density of galaxies with luminosity $> L_{UV}$ to match the number density of halos with mass $> M_h$. Formally,

$$\int_{M_{UV}} \Phi(M'_{UV}, z) dM'_{UV} = \int_{M_h} \frac{dn}{dM'_h} dM'_h, \quad (1)$$

where Φ is the UV LF at 1600 \AA and we use the Schechter parameterization with the redshift-dependent fitting parameters given in Bouwens et al. (2015). As a reference, in the derived $L_{UV} - M_h$ relations our minimum mass $5 \times 10^8 M_\odot$ corresponds to an absolute magnitude $M_{UV} = -10.5, -12.1, -13.0$ at $z = 5, 8, 10$ respectively. Luminosity

² http://homepage.sns.it/mesinger/DexM__21cmFAST.html

at other UV wavelengths is obtained through the luminosity-dependent Spectral Energy Distribution (SED) slope β (i.e., $f_\lambda \propto \lambda^\beta$) in Bouwens et al. (2014)³. However, generally speaking this power-law only holds at $\lambda \lesssim 2000 - 3000 \text{ \AA}$, while we need luminosities at least until $4.5/(1+z) \mu\text{m}$, say 7500 \AA when $z = 5$. Therefore at $\lambda > 2000 \text{ \AA}$ we use the SED template from Starburst99⁴ (Leitherer et al. 1999; Vázquez & Leitherer 2005; Leitherer et al. 2010), adopting a continuous star formation mode, with metallicity 0.1 Z_\odot and 200 Myr stellar age. The SB99 SEDs are normalized to match the power-law form at 2000 \AA .

The flux received in each pixel in the map is the sum of radiation from all galaxies seen by the pixel,

$$F(\nu_0) = \nu_0 \frac{1}{(\theta_{\text{pix}})^2} \sum_j \frac{L^j(\nu)(1+z_j)}{4\pi r_j^2(1+z_j)^2}, \quad (2)$$

where $\nu = \nu_0(1+z_j)$, z_j is the redshift of the j -th halos⁵ in the solid angle $(\theta_{\text{pix}})^2$ (we adopt $\theta_{\text{pix}} = 3.6''$ for all mock maps in this work), r_j is its comoving distance. In Fig. 1 we show the $3.6 \mu\text{m}$ flux map (bottom left panel) from all galaxies between $z = 5 - 10$ (flux from galaxies at $z > 10$ is negligible compared with galaxies at lower redshift, we ignore it here).

Finally, we construct the flux map of LBGs at $5 < z < 10$. To take into account selection effects, we assume a completeness function of the form

$$f(m) = 0.5[1 - \text{erf}(m - m_{\text{lim}})], \quad (3)$$

where erf is the error function, and m_{lim} is the limiting magnitude. When constructing the flux map, for each LBG with apparent magnitude m , we generate an uniformly distributed number x_r . Flux from these galaxies is added to the map only if $x_r \leq f(m)$. In Fig. 1 we show the $1.6 \mu\text{m}$ ⁶ flux map constructed from the LBGs for H -band limiting magnitudes $H_{\text{lim}} = 25$ (top left) and $H_{\text{lim}} = 27$ (top right) respectively.

2.2 NIRB contamination maps

In addition to the flux from high- z ($z > 5$) galaxies, the observed NIRB also contains radiation from unresolved, low- z galaxies, and an excess radiation from unknown sources (Yue et al. 2013b, 2014; Cooray et al. 2012b; Zemcov et al. 2014). We collectively refer to these two components as *contamination*, since in this work the targeted signal is

³ $\beta = \beta_{-19.5} + \frac{d\beta}{dM_{\text{UV}}}(M_{\text{UV}} + 19.5)$, the values of $\beta_{-19.5}$ and $\frac{d\beta}{dM_{\text{UV}}}$ at $z = 4, 5, 6$ and 7 could be found in Bouwens et al. (2014). For convenience of using this form at in-between redshifts, we fit z -dependent forms (Yue et al. 2015): $\beta_{-19.5} = -1.97 - 0.06(z - 6)$ and $\frac{d\beta}{dM_{\text{UV}}} = -0.18 - 0.03(z - 6)$. We use these fittings anyway when $5 < z < 10$.

⁴ <http://www.stsci.edu/science/starburst99/docs/default.htm>

⁵ We do not model photometric redshift uncertainties, because the redshift range considered here $z = 5 - 10$ is much larger than the uncertainties.

⁶ In this paper we only discuss the $1.6 \mu\text{m}$ flux maps of LBGs, because we consider a redshift range from $z = 5$ to 10 . For shorter wavelengths all procedures (and conclusions) are similar, with the only exception of a slightly smaller signal due to the Lyman dropout of $z \gtrsim 8$ galaxies.

the flux from high- z galaxies. To model such contaminating signal we construct random maps with mean flux 1.0 (0.7) $\text{nWm}^{-2}\text{sr}^{-1}$ at 3.6 (4.5) μm and reproduce the sum of (i) the angular power spectrum of the power *excess* (see Yue et al. 2013b) matching available observations (Cooray et al. 2012b; Kashlinsky et al. 2012), and (ii) the angular power spectrum of low- z galaxies (Helgason et al. 2012) producing shot noise level matching Kashlinsky et al. 2012 ($P_{\text{SN}} = 4.8 \times 10^{-11} \text{ nW}^2 \text{ m}^{-4} \text{ sr}^{-1}$ at $3.6 \mu\text{m}$ and $P_{\text{SN}} = 2.2 \times 10^{-11} \text{ nW}^2 \text{ m}^{-4} \text{ sr}^{-1}$ at $4.5 \mu\text{m}$, the corresponding subtraction magnitude is ~ 25 mag). The steps are:

- A white noise map, i.e. a Gaussian random field, is generated.
- This map is then transformed into spatial-frequency space by FFT.
- For each complex number in frequency space, its modulus is rescaled to be $\sqrt{P(q)}$, where P is the given power spectrum and q is the spatial-frequency. The zero-frequency ($q = 0$) element is set to be the mean flux.
- The above map is then transformed back into real space by inverse FFT, resulting in a synthetic image with the same 2-point clustering properties as the measured $P(q)$.

In Fig. 1 we plot a single realization of the contamination map at $3.6 \mu\text{m}$ as an example (bottom right). The contamination is not correlated with the high- z galaxy component; however, it adds noise to the cross-correlation signal. To account for the statistical variance of the contamination, we make 30 independent realizations. In Fig. 2 we show the angular power spectrum of bottom panels in Fig. 1. All maps are convolved with a circular symmetric *Spitzer* PSF before further analysis.

3 CROSS-CORRELATION OF LBGs AND NIRB

3.1 the correlation coefficient

We first analyze the correlation coefficient between the LBG flux map and the NIRB map. It is defined as

$$\mathcal{R} = \frac{\langle \delta F_{1.6} \delta F_{\lambda_0} \rangle}{\sqrt{\langle \delta F_{1.6}^2 \rangle \langle \delta F_{\lambda_0}^2 \rangle}}, \quad (4)$$

where λ_0 refers to either $3.6 \mu\text{m}$ or $4.5 \mu\text{m}$, $\delta F_{1.6}$ and δF_{λ_0} are the flux fluctuations of the same pixel (zero lag) at those two wavelengths. The brackets refer to the pixel-averaged fluctuations. The correlation coefficient indicates the fraction of sources contributing to common signals. Before calculating the correlation coefficient we smooth both the NIRB maps and the LBG flux maps by a real space top-hat window function with diameter $\theta = 10''$. This is to suppress the instrumental noise since in the measured NIRB maps (Kashlinsky et al. 2012) the instrumental noise is negligible at $\theta \gtrsim 10''$. The smoothing is not related to the LBG detection limits since it is performed on maps constructed from LBGs already present in catalogs. To mimic surveys with different areas, we cut out sub-maps with different areas from the full map. We choose three areas: $(0.036)^\circ$, $(0.3)^\circ$ and $(1.2)^\circ$ deg^2 , representing a survey region similar to HUDF/XDF, UDS, and an hypothetical larger field, respectively.

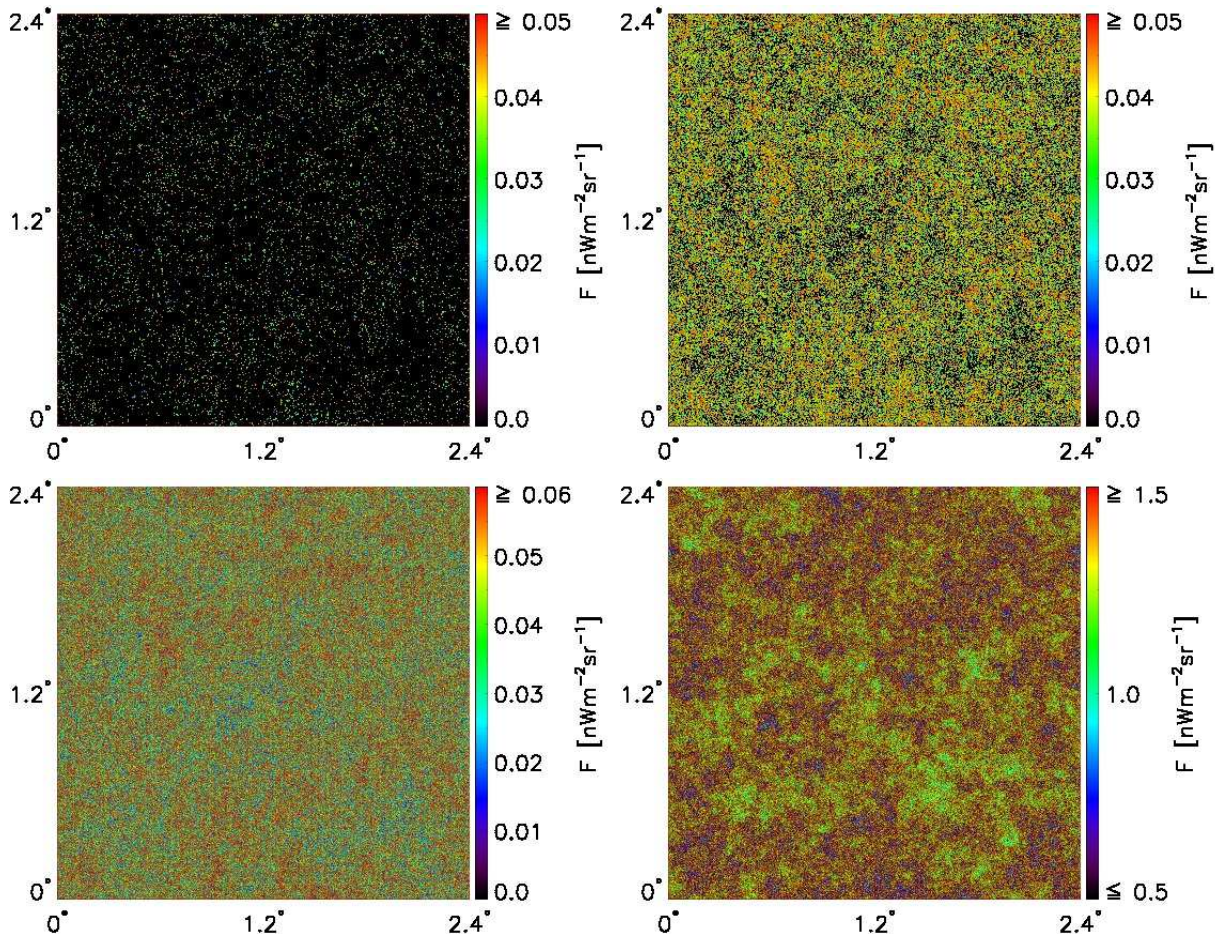


Figure 1. *Upper:* The $1.6 \mu\text{m}$ flux map constructed from resolved LBGs with $H_{\text{lim}} = 25$ (left) and $H_{\text{lim}} = 27$ (right) respectively. *Lower:* Map of the $3.6 \mu\text{m}$ flux from galaxies with $5 < z < 10$ (left) and map of contamination at the same wavelength (right). The mean flux of the latter is $1 \text{ nWm}^{-2}\text{sr}^{-1}$.

Before calculating the correlation coefficient, in both maps we mask pixels containing galaxies brighter than $\text{mag} \sim 25$ at *either* $3.6 \mu\text{m}$ or $4.5 \mu\text{m}$. From this procedure we obtain the source-subtracted NIRB map. The correlation coefficient vs. LBG limiting magnitude is shown in Fig. 3. The filled regions contain 68.3% probability of all sub-map samples. Note that we have 30 random realizations for each full map ($(2.4)^2 \text{ deg}^2$), so even for the $(1.2)^2 \text{ deg}^2$ case there are 120 samples, sufficient to compute the correlation coefficient variance.

Fig. 3 shows that it is indeed feasible to detect the cross-correlation signal from the mock maps, even for a relatively shallow survey with $H_{\text{lim}} \sim 25$, for which $\mathcal{R} \approx 0.04$. By pushing the limiting magnitude to fainter values, the correlation coefficient rapidly increases by a factor ~ 2 , and then slowly approaches ≈ 0.09 at $H_{\text{lim}} \sim 29$. It is worth noting that in small fields the measured correlation coefficient has a $\sim 30 - 80\%$ relative field-by-field scatter for $H_{\text{lim}} \gtrsim 26$, and even larger scatter at $H_{\text{lim}} < 26$. In some extreme cases there would be no or negative cross-correlation detected, due to the small number of LBGs contained in the fields.

To elucidate the differential contribution of LBGs, for a $(0.3)^2 \text{ deg}^2$ field, we further show in Fig. 4 the correlation coefficient from LBGs at $> z$ for $H_{\text{lim}} = 25, 26$ and 27 ,

respectively. For example, LBGs at $z > 8$ contribute $\mathcal{R} \approx 0.01$ at $H \lesssim 27$.

Our results are for NIRB maps with a fixed shot noise level matching Kashlinsky et al. (2012) measurements. Since the shot noise is mainly from low- z galaxies, an increased subtraction depth implies a relatively larger number of low- z galaxies (with respect to the high- z ones) are resolved and removed. As a result we expect a higher correlation coefficient. On the other hand, if we resolve more LBGs, the cross-power signal also becomes stronger. Thus, the strength of the cross-power signal vs. different LBGs detection depths can be used to determine the differential contribution of early galaxies.

3.2 Detectability vs. scales

So far we have investigated the behavior of the correlation coefficient by at a specific smoothing scale $\theta = 10''$. We now examine its dependence on angular scale. To this aim we re-define the correlation coefficient in the spatial-frequency domain via the power spectrum

$$\mathcal{R}_q(\theta) = \frac{P_{\text{IR} \times \text{G}}(\theta)}{\sqrt{P_{\text{IR}}(\theta) \times P_{\text{G}}(\theta)}}, \quad (5)$$

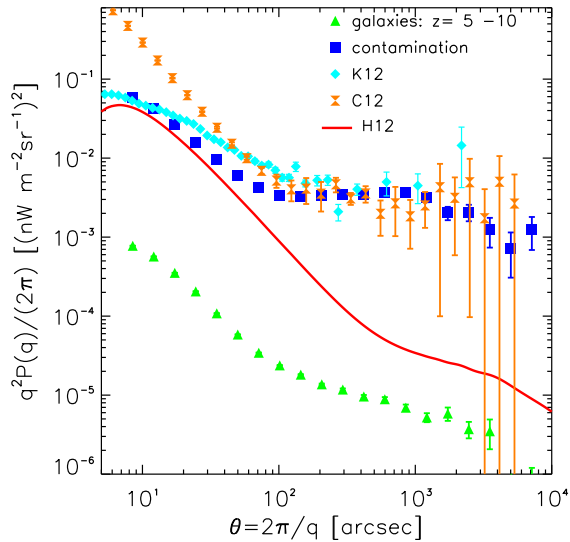


Figure 2. Angular power spectrum of the $3.6 \mu\text{m}$ flux map for $5 < z < 10$ galaxies (triangles) and contamination (squares). Errorbars show uncertainties due to limited number of Fourier modes in each q bin. As a comparison, in the same panel we also plot the Helgason et al. (2012) model for $z < 5$ galaxies (solid line), and the observational points in Kashlinsky et al. (2012) (diamonds) and Cooray et al. (2012b) (hourglasses). On large scales ($\theta \gtrsim 100''$) the angular power spectrum of our co-added map (quite similar to squares in the panel) is consistent with both observations. Compared with K12, at $\theta \lesssim 100''$ our prediction slightly falls short, probably because the non-linear clustering of low- z galaxies is not modeled here. The C12 observations have a shallower (i.e. ~ 24 mag) source subtraction, hence a higher shot-noise level.

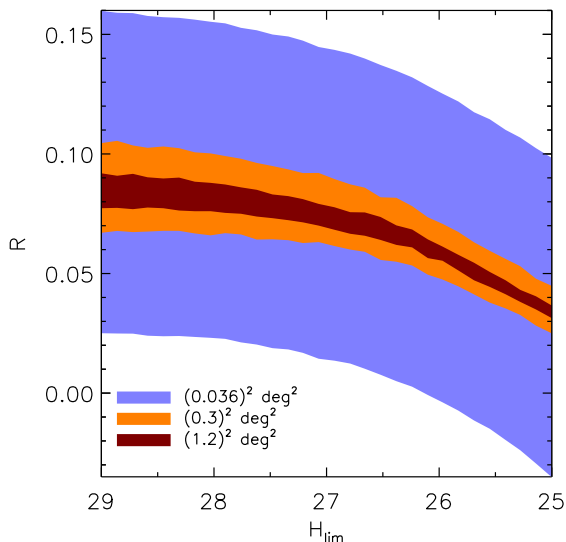


Figure 3. Correlation coefficient between the $3.6 \mu\text{m}$ source-subtracted NIRB and LBG flux maps vs. H -band limiting magnitudes for three different map areas. Filled regions bracket the 68.3% probability ranges around the peaks. All fields are smoothed on scale $\theta = 10''$.

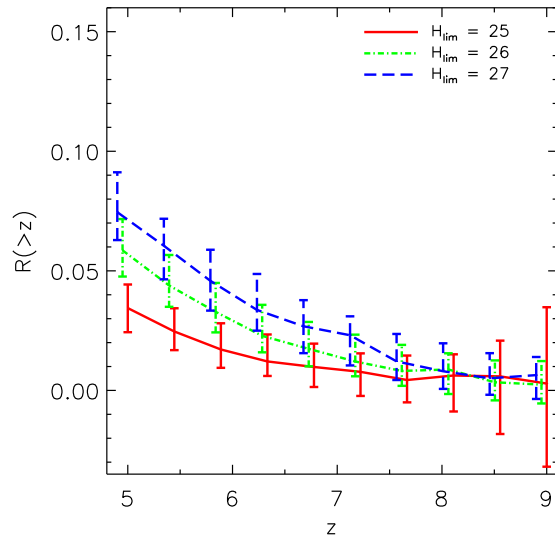


Figure 4. Contribution to correlation coefficient from LBGs with $> z$. The 68.3% probability ranges are plotted by errorbars. For displaying purpose we slightly shift the x-positions of some curves.

where $P_{1 \times 2}(\theta)$ is the cross-power spectrum and P_1, P_2 are the auto-power spectra. They are all calculated using the 2D FFT. Since $\delta F^2 \simeq q^2 P / 2\pi$, $\mathcal{R}_q \sim \mathcal{R}$ for the same θ . First we derive the shot noise due to LBGs fainter than a given H -magnitude (Fig. 5). It is the value of P_G taken on a sufficiently small scale $\theta \approx 14''$ (a stability check of the results for scales up to $\approx 40''$ has been performed). As we will point out in the following, shot noise is the most important term contributing to the cross-correlation. The shot noise level shown here is a useful reference for possible follow-up work on real data.

The $\mathcal{R}_q(\theta)$ between the source-subtracted NIRB at $3.6 \mu\text{m}$ and the $1.6 \mu\text{m}$ flux map of LBGs with $H_{\text{lim}} = 25, 26$ and 27 is shown by Fig. 6. The errorbars are the r.m.s of 30 samples each one using different random contamination realizations.

The cross-power spectrum includes both the shot noise and clustering terms. Shot noise is from sources common to both NIRB and LBG flux, and it is dominant on scales $\theta \lesssim 100''$. On larger scales, the clustering term progressively takes over. This term arises from all sources sharing the same large scale structure, including galaxies even fainter than the LBG limiting magnitude. As a consequence, in principle the clustering term could allow the detection of fainter galaxies in the source-subtracted NIRB through the cross-correlation with relatively bright LBGs. However, as shown by Fig. 6 the cross-correlation is more easily detected on small scales. Although the clustering term may contain more information, the main difficulty to be overcome in order to efficiently use this strategy is that even for a relatively large survey area of $(2.4)^2 \text{ deg}^2$ (i.e. our full map), the signal-to-noise ratio never exceeds ~ 3 at $\theta \gtrsim 300''$ for $H_{\text{lim}} < 27$. While increasing the limiting magnitude to > 27 does not help much to this aim, the noise could be reduced by using larger survey areas, as expected with, e.g. EUCLID and WFIRST.

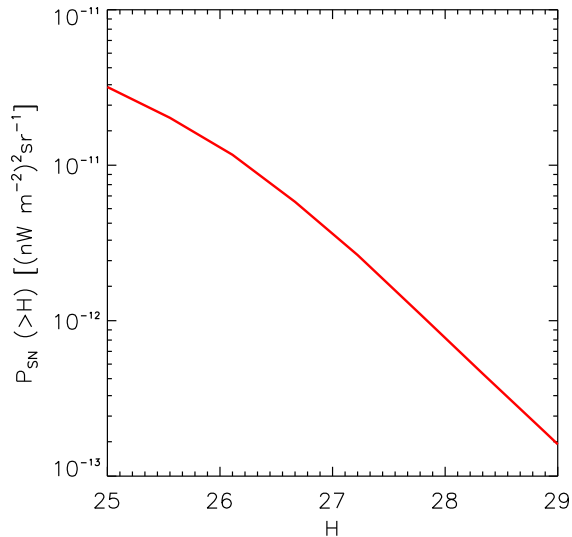


Figure 5. Shot noise due to LBGs with magnitude $> H$ and at $5 < z < 10$.

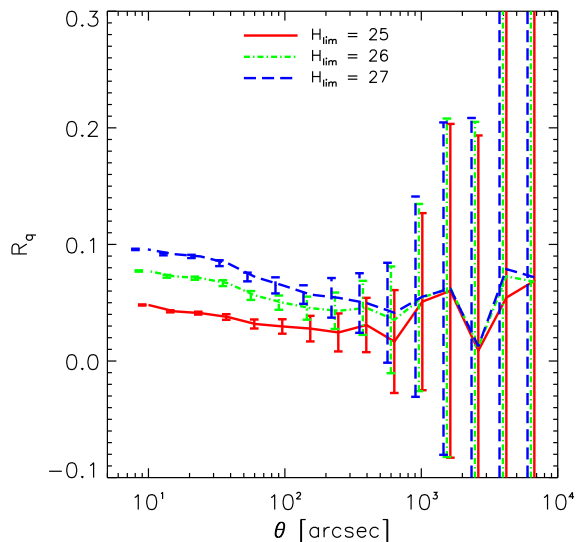


Figure 6. The \mathcal{R}_q between the source-subtracted NIRB and the flux maps constructed from LBGs with different H_{lim} . The error bars here show the r.m.s of 30 random realizations. For displaying purpose we slightly shift the x-positions of $H_{\text{lim}} = 26, 27$ curves.

3.3 Colors

From our mock maps it is also possible to characterize the colors, i.e. the ratio between flux in two bands, of unresolved galaxies in NIRB observations. With the assumption

$$\frac{F_{4.5}}{F_{3.6}} \approx \frac{\langle (\delta F_{4.5} \delta F_{1.6})_{\theta} \rangle}{\langle (\delta F_{3.6} \delta F_{1.6})_{\theta} \rangle}, \quad (6)$$

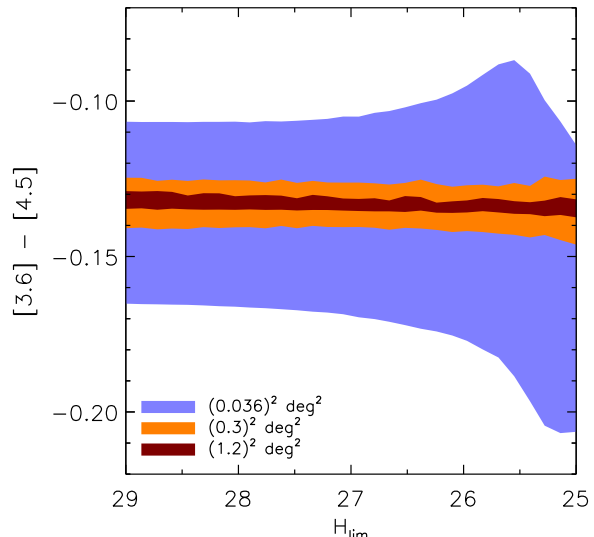


Figure 7. The magnitude difference, $[3.6] - [4.5]$, of fluctuations due to unresolved galaxies in the source-subtracted NIRB maps as a function of the survey limiting magnitude. Filled regions indicate 68.3% probability ranges.

we derive the magnitude difference as

$$\begin{aligned} [3.6] - [4.5] &= 2.5 \log \left(\frac{4.5 F_{4.5}}{3.6 F_{3.6}} \right) \\ &\approx 2.5 \log \left(\frac{4.5 \langle (\delta F_{4.5} \delta F_{1.6})_{\theta} \rangle}{3.6 \langle (\delta F_{3.6} \delta F_{1.6})_{\theta} \rangle} \right) \end{aligned} \quad (7)$$

Such magnitude difference, which might considerably vary for individual galaxies, represents the combined and weighted color of the unresolved galaxy population in these bands. In practice the PSF adds a bias to the measured flux ratio. Therefore before calculating the magnitude difference it would be necessary to first deconvolve the PSF from each map. We skip this step here and directly calculate the magnitude difference on maps without PSF convolution. Again we specify $\theta = 10''$. The predicted color as a function of H_{lim} is reported in Fig. 7, allowing us to conclude that the magnitude difference which is ~ -0.13 mag, could be detected by cross-correlating survey maps with area $\gtrsim (0.3)^2 \text{ deg}^2$. The figure reiterates that smaller area fields would be affected by bias effects.

4 CONCLUSIONS

Motivated by the fact that LBG surveys carried out by the *HST* have reached detection limits much deeper than the NIRB measured by *Spitzer* at longer wavelengths, in this paper we investigated the feasibility to pick the resolved LBGs component out of the NIRB by a cross-correlation analysis. Our investigations were based on mock maps constructed from semi-numerical simulations of halo formation, and empirically determined $L_{\text{UV}} - M_{\text{h}}$ relations.

We found that in the NIRB observed at 3.6 and 4.5 μm and with sources subtracted down to ~ 25 apparent magnitude, at smallest scales where the shot noise dominates,

about 10% of the flux fluctuations arises from LBGs in $5 < z < 10$ and with $H \lesssim 29$. Such faint galaxies have already been resolved in the existing deep surveys. However, this fractional contribution, if measured from narrow fields with area $\sim (0.036)^2 \text{ deg}^2$ (as the HUDF/XDF), could vary from $\sim 3\%$ to $\sim 16\%$. If the limiting magnitude is decreased to $H \sim 27$, the fractional contribution decreases to about 8%. If in this case we consider a larger field, e.g. with area similar to the UDS ($\sim (0.3)^2 \text{ deg}^2$), then the correlation coefficient varies in the narrower range $\sim 6\% - 9\%$. We remind that the variance at hand here is due to both the large-scale inhomogeneity of the signal and the contamination: it is the field-to-field variance of the correlation itself. We do not model errors introduced by data analysis procedures, as for example mask effects. However, at least theoretically we have shown that the contribution from the faintest galaxies could be isolated from the NIRB through the cross-correlation analysis.

We pointed out that it is still challenging to use the cross-correlation arising from the clustering term of the cross-power spectrum to study galaxies unresolved not only in NIRB observations, but also in LBG surveys. This term is dominant at $\gtrsim 200''$, but even for survey areas as large as $(2.4)^2 \text{ deg}^2$, the signal has a small significance, with a S/N ratio $\lesssim 3$. Although very unlikely, if the NIRB clustering excess originates from LBGs we would detect a correlation coefficient close to 1 at scales where the clustering term dominates. Stated differently, a measured correlation coefficient $\mathcal{R} \ll 1$ would actually rule out this scenario.

Our results have interesting implications also for the colors of high- z galaxy population. The colors of LBGs detected at wavelengths $< 1.6 \mu\text{m}$ but too faint to be individually resolved by existing telescopes at 3.6 and $4.5 \mu\text{m}$, can be obtained by using the cross-correlation with the NIRB in these two longer wavelength bands.

It is worth noting that the predictions presented in this paper assume a contaminating signal in the form of NIRB fluctuation excess which originates from direct collapse black holes at high z (Yue et al. 2013b). If however the excess is found to arise more locally, we might be able to model or subtract it more accurately, thereby making the signal calculated in this paper more easily detectable, i.e. $\langle \mathcal{R} \rangle \gtrsim 0.1$.

Importantly, the study proposed here can be further developed to infer the properties of even fainter high- z galaxy populations that are currently inaccessible to direct telescopic detection. This could, for example, be accomplished by a Lyman-break tomography study designed to isolate high- z populations via multi-band cross-correlations without requiring prior LBG detections (Kashlinsky et al. 2015).

ACKNOWLEDGMENTS

We thank A. Kashlinsky for valuable comments on the manuscript.

REFERENCES

Arendt R. G., Kashlinsky A., Moseley S. H., Mather J., 2010, ApJS, 186, 10
 Atrio-Barandela F., Kashlinsky A., 2014, ApJ, 797, L26

Blaizot J., Wadadekar Y., Guiderdoni B., Colombi S. T., Bertin E., Bouchet F. R., Devriendt J. E. G., Hatton S., 2005, MNRAS, 360, 159
 Bouwens R. J. et al., 2011, ApJ, 737, 90
 Bouwens R. J. et al., 2014, ApJ, 793, 115
 Bouwens R. J. et al., 2015, ApJ, 803, 34
 Cappelluti N. et al., 2013, ApJ, 769, 68
 Choudhury T. R., Ferrara A., 2007, MNRAS, 380, L6
 Cooray A., Bock J. J., Keatin B., Lange A. E., Matsumoto T., 2004, ApJ, 606, 611
 Cooray A., Gong Y., Smidt J., Santos M. G., 2012a, ApJ, 756, 92
 Cooray A. et al., 2012b, Nature, 490, 514
 Cooray A. et al., 2007, ApJ, 659, L91
 Cooray A., Yoshida N., 2004, MNRAS, 351, L71
 Fernandez E. R., Dole H., Iliev I. T., 2013, ApJ, 764, 56
 Fernandez E. R., Iliev I. T., Komatsu E., Shapiro P. R., 2012, ApJ, 750, 20
 Fernandez E. R., Komatsu E., 2006, ApJ, 646, 703
 Fernandez E. R., Komatsu E., Iliev I. T., Shapiro P. R., 2010, ApJ, 710, 1089
 Fernandez E. R., Zaroubi S., 2013, MNRAS, 433, 2047
 Fernandez E. R., Zaroubi S., Iliev I. T., Mellema G., Jelić V., 2014, MNRAS, 440, 298
 Helgason K., Ricotti M., Kashlinsky A., 2012, ApJ, 752, 113
 Helgason K., Ricotti M., Kashlinsky A., Bromm V., 2016, MNRAS, 455, 282
 Illingworth G. D. et al., 2013, ApJS, 209, 6
 Kashlinsky A., Arendt R., Gardner J. P., Mather J. C., Moseley S. H., 2004, ApJ, 608, 1
 Kashlinsky A., Arendt R. G., Ashby M. L. N., Fazio G. G., Mather J., Moseley S. H., 2012, ApJ, 753, 63
 Kashlinsky A., Arendt R. G., Mather J., Moseley S. H., 2005, Nature, 438, 45
 Kashlinsky A., Arendt R. G., Mather J., Moseley S. H., 2007a, ApJ, 666, L1
 Kashlinsky A., Arendt R. G., Mather J., Moseley S. H., 2007b, ApJ, 654, L5
 Kashlinsky A., Arendt R. G., Mather J., Moseley S. H., 2007c, ApJ, 654, L1
 Kashlinsky A., Mather J. C., Helgason K., Arendt R. G., Bromm V., Moseley S. H., 2015, ApJ, 804, 99
 Kashlinsky A., Odenwald S., Mather J., Skrutskie M. F., Cutri R. M., 2002, ApJ, 579, L53
 Leitherer C., Ortiz Otálvaro P. A., Bresolin F., Kudritzki R.-P., Lo Faro B., Pauldrach A. W. A., Pettini M., Rix S. A., 2010, ApJS, 189, 309
 Leitherer C. et al., 1999, ApJS, 123, 3
 Magliocchetti M., Salvaterra R., Ferrara A., 2003, MNRAS, 342, L25
 Mao X.-C., 2014, ApJ, 790, 148
 Matsumoto T. et al., 2005, ApJ, 626, 31
 Matsumoto T. et al., 2011, ApJ, 742, 124
 Mesinger A., Furlanetto S., 2007, ApJ, 669, 663
 Oke J. B., Gunn J. E., 1983, ApJ, 266, 713
 Planck Collaboration et al., 2014, A&A, 571, A16
 Raičević M., Theuns T., Lacey C., 2011, MNRAS, 410, 775
 Salvaterra R., Ferrara A., 2003, MNRAS, 339, 973
 Salvaterra R., Ferrara A., 2006, MNRAS, 367, L11
 Salvaterra R., Ferrara A., Dayal P., 2011, MNRAS, 414, 847
 Salvaterra R., Magliocchetti M., Ferrara A., Schneider R., 2006, MNRAS, 368, L6
 Santos M. R., Bromm V., Kamionkowski M., 2002, MNRAS, 336, 1082
 Seo H. J., Lee H. M., Matsumoto T., Jeong W.-S., Lee M. G., Pyo J., 2015, ArXiv e-prints, 1504.05681
 Thompson R. I., Eisenstein D., Fan X., Rieke M., Kennicutt R. C., 2007, ApJ, 657, 669
 Vázquez G. A., Leitherer C., 2005, ApJ, 621, 695

- Yue B., Ferrara A., Pallottini A., Gallerani S., Vallini L., 2015, MNRAS, 450, 3829
- Yue B., Ferrara A., Salvaterra R., Chen X., 2013a, MNRAS, 431, 383
- Yue B., Ferrara A., Salvaterra R., Xu Y., Chen X., 2013b, MNRAS, 433, 1556
- Yue B., Ferrara A., Salvaterra R., Xu Y., Chen X., 2014, MNRAS, 440, 1263
- Zemcov M. et al., 2014, Science, 346, 732